

1           **Capturing the Little Washita Watershed Water**  
2           **Balance with a Physically-Based**  
3           **Two-Hydrologic-Variable Model**

4           **Fanny Picourlat<sup>1</sup>, Emmanuel Mouche<sup>1</sup>, Claude Mügler<sup>1</sup>**

5           <sup>1</sup>Laboratoire des Sciences du Climat et de l'Environnement, LSCE/IPSL, CEA-CNRS-UVSQ, Université  
6           Paris-Saclay, Gif-sur-Yvette, France

7           **Key Points:**

- 8           • An upscaling approach reduces model dimensionality from 3D watershed, to 2D  
9           equivalent hillslope, to a two-hydrologic-variable model  
10          • The approach is developed on the 20-year hydrology (1993-2013) of the Little Washita  
11          Watershed (Ok, USA)

---

Corresponding author: Fanny Picourlat, [fanny.picourlat@lsce.ipsl.fr](mailto:fanny.picourlat@lsce.ipsl.fr)

12 **Abstract**

13 Land Surface Models (LSMs) are key components of Earth System Models (ESMs)  
 14 for which the Intergovernmental Panel on Climate Change (IPCC) studies rely on. How-  
 15 ever, these models either neglect or conceptually represent the basin-scale hydrologic pro-  
 16 cesses that produce the land surface water balance. One challenge is to bring the dom-  
 17 inant physical processes from the local scale up to the LSMs. It requires a synergy be-  
 18 tween two communities working with two different approaches: the hydrology and the  
 19 LSMs modeling communities. As local-scale hydrologists, we here present an upscaling  
 20 (or bottom-up) approach that aims to identify the basin-scale driving variables that need  
 21 to be exported into LSMs. The approach is developed on the Little Washita Watershed  
 22 (Ok, USA) 20-year hydrology (1993-2013). A 3D physically-based model, built with Hy-  
 23 droGeoSphere, first produces a reference simulation. An equivalent hillslope model is then  
 24 able to capture both 3D simulated water balance and local water table dynamics with  
 25 good accuracy. Physical analysis of the water balance in the different hillslope compart-  
 26 ments leads to the identification of two driving variables: seepage face extension and wa-  
 27 ter table slope. They are then implemented in an analytical physically-based model. Re-  
 28 sults show a good capacity of this model to capture the water balance of hillslopes hav-  
 29 ing different lengths and slopes. Moreover, it is able to capture the water balance of the  
 30 equivalent hillslope, and therefore of the watershed, over the 20-year period with good  
 31 accuracy. In this manner, the proposed approach reduces the 3D watershed model to a  
 32 two-variable analytical model.

33 **1 Introduction**

34 Land Surface Models (LSMs) are key components of the Earth System Models (ESMs)  
 35 used in the studies of past and future global evolution. In order to increase LSMs per-  
 36 formance, authors converge on the need to improve the representation of land surface  
 37 processes, including hydrologic processes (Clark et al., 2015; Fan et al., 2019; Fisher &  
 38 Koven, 2020). To meet this challenge, a joint effort is needed from two modeling com-  
 39 munities: the hydrology and the LSMs modeling communities.

40 The hydrology modeling community usually work at the local to regional basin scale  
 41 (i.e.  $< 10^3 \text{ km}^2$ ). The basin constitutes the basic unit for the study of hydrologic pro-  
 42 cesses. Moreover the physically-based modeling approach is commonly used at this scale.  
 43 Since it has been introduced by the blueprint of Freeze and Harlan (1969), this approach  
 44 has been largely developed in the community with the appearance of several models: CATHY  
 45 (Bixio et al., 2002; Camporese et al., 2010), ParFlow (Maxwell et al., 2009), HydroGeo-  
 46 Sphere (Therrien et al., 2010), etc. They constitute a major tool for dynamically sim-  
 47 ulating surface water and groundwater flows and interactions, and for understanding the  
 48 physics behind local hydrologic processes. For instance, Kollet and Maxwell (2008) show  
 49 the impacts of groundwater dynamics on the surface energy balance using Parflow, or  
 50 Scudeler et al. (2017) study the evolution of the seepage face located at the intersection  
 51 between saturated zone and soil surface using CATHY. However, considering the cur-  
 52 rently existing computational resources, their level of complexity make their application  
 53 to larger scale very challenging, if not impossible. Maxwell et al. (2015) are the first to  
 54 conduct a continental-scale simulation using an integrated physically-based model with  
 55 high discretization. Although this work demonstrates the feasibility of such an approach,  
 56 the conducted steady-state simulation requires significant computational resources, and  
 57 a transient one would be even more expensive.

58 On another hand, the LSMs community uses a simplified hydrologic modeling ap-  
 59 proach as component of the LSMs in order to simulate continental hydrology while keep-  
 60 ing the models tractable at the global scale (e.g. Nijssen et al., 1997; Rosnay & Polcher,  
 61 1998; Bonan et al., 2002; Milly et al., 2014). LSMs are built on coarse grid cells (20 to  
 62 200 km horizontal resolution) and consider only one dimensional vertical fluxes through

63 a few meters of soil. Since local processes driven by lateral gradients are neglected, the  
 64 physical reality of these models is questionable. As a result, their ability to accurately  
 65 capture global water balance evolution within a changing climate also is uncertain. Ac-  
 66 cording to Clark et al. (2015), LSMs hydrology should benefit from local processes un-  
 67 derstanding in basin scale hydrology. However, one challenge is to create bridges between  
 68 two communities working with two different modeling approaches, and to develop meth-  
 69 ods for exporting local physical processes into global scale models without increasing their  
 70 computational cost.

71 Some authors have started to build these bridges. Maquin et al. (2017) introduce  
 72 the Hydrologic Hillslope-based Soil Column model (H2SC) which is a 1D soil column model  
 73 that simulates both vertical flow and lateral flow through respectively the Richards equa-  
 74 tion and a drainage function based on simplified hillslope hydrology. H2SC model allows  
 75 the simulation of water table dynamics and its impact on the evapotranspiration fluxes.  
 76 The influence of groundwater bodies on evapotranspiration fluxes, whose significance is  
 77 demonstrated in particular by Kollet and Maxwell (2008), is not accounted in LSMs since  
 78 they do not explicitly account for water table dynamics and lateral flows. In that respect,  
 79 the H2SC model is an interesting approach for the representation of these processes in  
 80 a one dimensional column model like LSMs. However H2SC is only applied on two piezome-  
 81 ter sites in the Strengbach catchment (France) and links between H2SC and LSMs are  
 82 not established. In the same vein, Hazenberg et al. (2015) present a relatively more com-  
 83 plex model: the hybrid-3D hillslope hydrologic model (h3D). It results from the coupling  
 84 of Richards equation, hillslope-storage Boussinesq equation (Troch et al., 2003) and dif-  
 85 fusive wave approximation for the simulation of respectively vertical, lateral subsurface  
 86 and lateral overland flows in a hillslope. The h3D model is tested on a numerical recharge-  
 87 drainage experiment and validated by comparing simulation results with a CATHY mod-  
 88 eling of the hillslope. Then, Hazenberg et al. (2016) validate the h3D model with recharge-  
 89 drainage experiment executed in Landscape Evolution Observatory hillslopes. Next step  
 90 is to implement h3D model into a LSM. However the ability of h3D model to capture  
 91 "real world" watershed water balance evolution is not assessed. Authors from the LSMs  
 92 community also develop strategies to implement lateral flows into their models. It is the  
 93 case for instance in the Community Land Model (CLM) (Swenson et al., 2019) or in the  
 94 Organizing Carbon and Hydrology in Dynamic Ecosystems model (ORCHIDEE) one (Tootchifatidehi,  
 95 2019; Verbeke et al., 2019). These approaches can be qualified as "top-down" since they  
 96 use large scale models as the starting point of their reasoning and then implement com-  
 97 plexity in order to account for smaller scale processes. Swenson et al. (2019) account for  
 98 lateral flow by dividing grid cells into HRUs, while ORCHIDEE modelers decompose each  
 99 grid cell into an upland and a lowland compartment.

100 As it is defended by Hrachowitz and Clark (2017) and Clark et al. (2017), we be-  
 101 lieve that hydrologic modeling, and more particularly hydrologic processes representa-  
 102 tion in global scale models, would benefit from being enriched by both top-down and bottom-  
 103 up approaches. As complementary work to the authors cited above, this study presents  
 104 a bottom-up approach also called upscaling approach. It aims to use a watershed physically-  
 105 based model as the starting point of the reasoning before zooming out by identifying key  
 106 variables to import into larger scales. This approach is developed on the Little Washita  
 107 Watershed (Ok, USA) with three modeling steps: First a three-dimensional simulation  
 108 of the basin's 20-year hydrology is conducted using the integrated code HydroGeoSphere  
 109 (HGS). This simulation constitutes the reference result for evaluating the upscaling ap-  
 110 proach of the watershed water balance. Then, the 3D water balance is simulated by us-  
 111 ing a two-dimensional equivalent hillslope model. Finally, the water balance analysis of  
 112 the hillslope compartments allows the conceptualization of its physical functioning. Two  
 113 driving variables are identified and used in physically-based laws forming an analytical  
 114 model. The resulting two-hydrologic-variable model aims to simulate the two outgoing  
 115 fluxes of the watershed water budget: runoff and evapotranspiration fluxes.

116 In the following section 2, the Little Washita Watershed (LWW) is presented along  
 117 with its geomorphic data and its 20-years climatic and hydrologic data. In section 3, the  
 118 three modeling steps are detailed. In section 4, the 3D simulated reference water-budget  
 119 is assessed with available experimental data, then the equivalent hillslope model results  
 120 are compared to the 3D reference ones, and finally the analytical model is qualified. Con-  
 121 clusions are drawn in section 5.

## 122 2 The Little Washita Watershed: 20 Years Climatic and Hydrologic 123 Evolution

124 Well known by the scientific community, the LWW is a study site where a lot of  
 125 experimental and numerical efforts have converged (Steiner et al., 2014). Indeed, sev-  
 126 eral measurement networks have been implemented (Starks, Steiner, & Stern, 2014) since  
 127 1960, allowing the record of meteorological data, soil temperature and soil moisture. In  
 128 parallel, the basin has been used as the study site of multiple modeling works (Van Liew  
 129 & Garbrecht, 2003; Rigon et al., 2006; Kollet & Maxwell, 2008; Ferguson & Maxwell, 2010;  
 130 Rosero et al., 2011; Condon & Maxwell, 2014; Chaney et al., 2016). As a rich set of stud-  
 131 ies has been conducted on this basin, the LWW is a great candidate for developing our  
 132 upscaling approach.

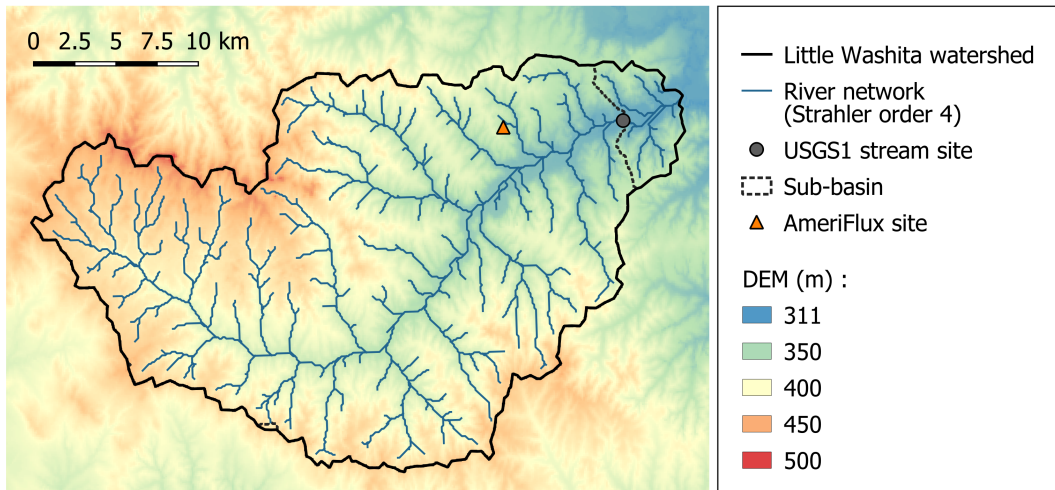


**Figure 1.** Topography and river network in the Little Washita Watershed. Location of two measurement sites: USGS 07327550 streamflow measurement station (referred to as USGS1 stream site) and AmeriFlux site for the measurement of surface energy balance components. The digital elevation model (DEM) is taken from USGS database and has a resolution of 100 m.

133 The watershed covers  $610 \text{ km}^2$  with maximum and minimum elevations of respec-  
 134 tively 493 m and 317 m above mean sea level (Figure 1). Its size is therefore in the range  
 135 of LSMs grid resolution. The distribution of two geomorphic characteristics (Horton, 1932)  
 136 is extracted from the 100 m resolution DEM and is plotted in Figure 2: the hillslopes  
 137 length and mean slope. The computed mean values are respectively 1200 m and 2%, what  
 138 reflects a smooth topography. The geology is composed by Permian age sedimentary rocks  
 139 (Allen & Naney, 1991) which underlie variably permeable soils ranging from fine sand  
 140 with saturated hydraulic conductivities around  $2 \times 10^{-5} \text{ ms}^{-1}$ , to silty loams with sat-  
 141 urated hydraulic conductivities around  $1 \times 10^{-6} \text{ ms}^{-1}$  (mean values for the main LWW  
 142 soil mapping units of the STATSGO database presented in Moriasi et al. (2014)). Ac-  
 143 cording to Starks, Steiner, and Stern (2014), 68% of the watershed is covered by grass-

144 land, 20% is used to grow crops, 8% is occupied by forests and the remaining 4% corresponds to urban areas and roads. They study land cover databases from the 1974 to  
 145 2007 and show that it remains quite stable.  
 146

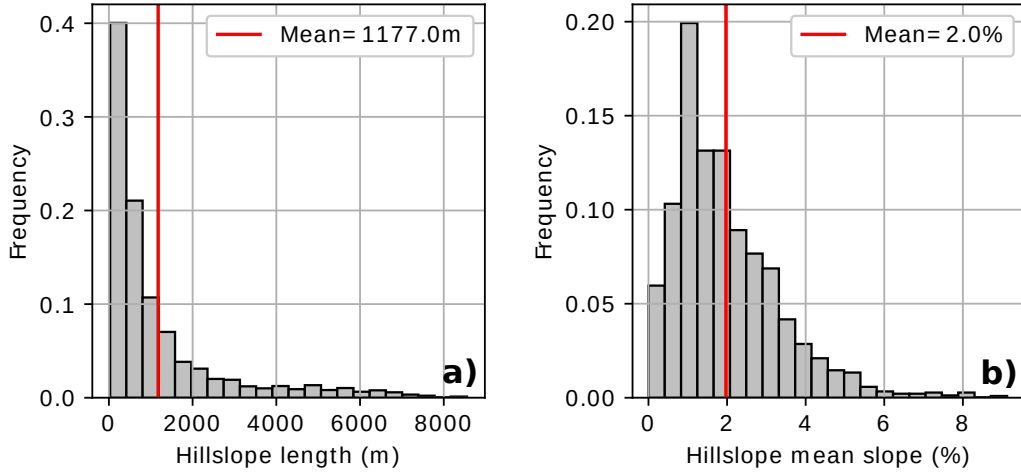


**Figure 2.** Geomorphic analysis of the LWW: (a) Hillslope length and (b) mean slope distribution over the basin. Analysis are conducted on the 100 m resolution DEM using a flow paths modeling algorithm (Maquin, 2016).

147 The climate is characterized by an annual mean rainfall rate around 800 mm and  
 148 an annual mean temperature of 15°C (“Caddo County climate summary” (2017), mean  
 149 value of Caddo County for the period 1981-2010). By analyzing long term climate data  
 150 record in the area, Garbrecht et al. (2014) show a 40-year rising trend in observed air  
 151 temperature starting in 1972. The temperature increases by 0.34°C per year, which is  
 152 interpreted as a sign of climate change. A fraction of this climatic evolution and its con-  
 153 sequences on the watershed hydrology can be observed in the 20-year period on which  
 154 we focus. Figure 3a shows the annual potential evapotranspiration (PET) and rainfall  
 155 rates over this period, based on North American Regional Reanalysis (NARR) dataset  
 156 which has spatial and temporal resolutions of 30 km and 3 hours, respectively (Mesinger  
 157 et al., 2006). PET increases while rainfall decreases, leading to a PET that is two to five  
 158 times greater than total precipitation. Regarding monthly means over the period (Fig-  
 159 ure 3c), the largest precipitation rates occur in April to June and September to Octo-  
 160 ber, while the largest PET rate occurs in July.

161 The LWW has been instrumented with streamflow measurement stations monitored  
 162 by the United States Geological Survey (USGS) since 1992. The more downstream one,  
 163 called here USGS1 (Figure 1), drains an area of 601 km<sup>2</sup>. Data at this station (Figures  
 164 3b and 3d) indicate a decreasing trend of the discharge over the period with high val-  
 165 ues in 1997-1998 and 2006-2007. The 2006-2007 peak corresponds to a year with a high  
 166 rainfall rate. However, the 1997-1998 peak might be due to rainfall timing. During this  
 167 water year, the largest rainfall events occurred in December to January while the poten-  
 168 tial evapotranspiration was minimum, thus producing peak flow rates. This year can be  
 169 qualified as particular, since peak rainfall and flow rates usually happen in April to June.

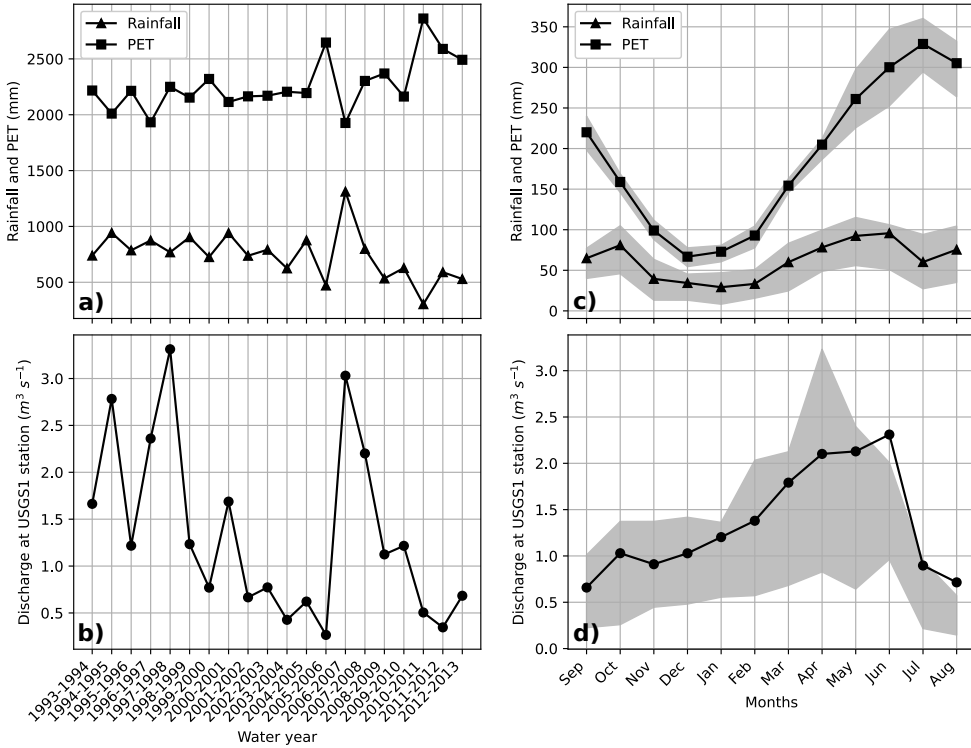


**Figure 3.** Evolution over the 20-year period of (a) annual potential evapotranspiration (PET) and rainfall, (b) annual discharge, (c) seasonal PET and rainfall, and (d) seasonal discharge. Seasonal evolutions are built with monthly averaged values over the 20-year period. The colored bands indicate the interval between first and third quartiles of interannual variability.

### 3 Hydrologic Models

A three-dimensional model of the LWW is first built and run over the twenty-year period of time. Since no water table depth measurement and only one-year local latent heat flux measurement are available on the basin, the aim is to have a continuous 3D view on the basin's hydrology that will serve as a reference. A 2D equivalent hillslope is then set up and compared to the reference result. Indeed the hillslope is considered as the main hydrologic unit controlling hydraulic gradients and main lateral flows within a catchment (Band, 1989; Fan & Bras, 1998; Khan et al., 2014; Loritz et al., 2017). Recently, the synthesis paper of Fan et al. (2019) reminded the importance of the hillslope scale in the water distribution over the landscape and water availability for evapotranspiration. The LWW 2D equivalent hillslope model is finally reduced to a two-variable analytical model.

Both 3D and 2D hydrologic models are built with HydroGeoSphere (HGS), which is a 3D fully integrated surface and subsurface simulator. It couples the diffusion-wave equation for 2D surface flow and Richards equation for 3D variably saturated subsurface flow using dual node approach. Flow equations are solved applying control volume finite element method with Newton-Raphson linearization technique. HGS includes adaptive time stepping options. The model is forced with rainfall and PET data. PET data delineate the maximum evapotranspiration rate. Actual evapotranspiration is then estimated considering three different limiting factors: Leaf area index (LAI), soil moisture

190 and root distribution (Kristensen & Jensen, 1975; Wigmosta et al., 1994). A complete  
 191 description of the HGS model and its governing equations is available in the literature  
 192 (Therrien et al., 2010).

### 193 3.1 The Three-Dimensional Model

194 The LWW three-dimensionnal mesh is constructed with a horizontal spatial dis-  
 195cretization ranging from 1 km to 100 m around the river network. This finer mesh around  
 196 the river network allows a precise representation of the rivers and of the processes oc-  
 197curring nearby. The topography is taken from the USGS DEM presented in section 2.  
 198 A flat limit is set at the bottom boundary of the model, resulting in a subsurface domain  
 199 whose depth ranges from 60 m to 214 m, as Kollet and Maxwell (2008) did for their LWW  
 200 model built with ParFlow. Vertical discretization is refined near the surface and becomes  
 201 coarser with depth: it ranges from 1 cm to a maximum of 18 m. This discretization re-  
 202 sults in 307097 elements and 163180 nodes. Regarding the temporal discretization, the  
 203 timestep is adaptative with a maximum value of one day.

204 A no flow boundary condition is applied to all boundaries of the domain, except  
 205 for the top boundary and the outlet of the Little Washita river where a critical depth  
 206 boundary condition allows the streamflow to exit the system. At the top boundary, the  
 207 model is forced with daily PET and rainfall from the NARR dataset previously presented  
 208 in section 2. The forcings are spatially uniform over the basin. Subsurface domain pa-  
 209 rameters are homogeneous and taken from Kollet and Maxwell (2008), except for the hy-  
 210draulic conductivity which was manually calibrated. Subsurface parameters are the fol-  
 211 lowing: Saturated hydraulic conductivity  $K = 5 \times 10^{-6} \text{ ms}^{-1}$ , porosity  $\theta_s = 0.4$ , resid-  
 212 ual saturation  $S_{wr} = 0.2$ , van Genuchten parameters  $\alpha = 3.5 \text{ m}^{-1}$  and  $\beta = 2.0$ . Sim-  
 213 ulation tests were conducted with distributed soil parameters based on Kollet and Maxwell  
 214 (2008) and specialized rainfall forcing taken from the local measurement network of Agri-  
 215 cultural Research Services (Starks, Fiebrich, et al., 2014). Complexity addition into the  
 216 model shows no consequences on the output streamflow. Consequently the choice is made  
 217 to work with homogeneous soil parameters and forcings. Regarding vegetation param-  
 218 eters, they are distributed according to USGS land cover dataset at a resolution of 100  
 219 m. A summary of subsurface, surface and evapotranspiration parameters (determined  
 220 from both literature and an ensemble of calibration work) is available with the simula-  
 221 tion datasets (see acknowledgments).

222 Initial conditions are obtained by using a spin-up method over one year. The 1993-  
 223 1994 water year is simulated over and over until an equilibrium state is reached. It is as-  
 224 sumed to happen when the variation of water volume in the subsurface becomes lower  
 225 than 0.2% of the initial water volume. At the beginning of the spin-up process, the wa-  
 226 ter table is set to 2 m under the surface. Then, nine spin-up simulations are needed to  
 227 reach the equilibrium state.

### 228 3.2 The Equivalent Hillslope Model

229 Since the objective of the model dimensionality reduction is the upscaling of the  
 230 processes, the reduced model must have a simple geometry in order to be easily concep-  
 231 tualisable. Consequently, the equivalent hillslope is built with a linear soil surface, what  
 232 results in a single slope parameter (Figure 4). It is defined by the soil surface angle tan-  
 233 gent:  $\tan(\gamma)$ . As for the 3D model, the bottom line is horizontal. The hillslope height  
 234 at  $x = 0$ , named  $h_r$ , equals 96 m. It corresponds to the mean subsurface depth below  
 235 the river network. The hillslope model is constructed with an horizontal spatial discretiza-  
 236 tion of 100 m, which is equal to the 3D one around the river network, and a vertical dis-  
 237 cretization also identical to the 3D one. The timestep is parametrized the same way.

Identical PET and rainfall forcings are used. A no flow boundary condition is applied at the lateral and bottom boundaries of the hillslope. The more downstream lateral boundary, located below the river network is considered as a symmetry plane. Consequently, a no flow condition is also applied. Discharge is modeled by water leaving the system through a critical depth boundary condition imposed at the more downstream surface nodes. This river representation through a subsurface no flow condition and a surface critical depth condition allows the representation of a dynamic seepage face  $X_s(t)$  where groundwater-surface water interaction participates in the generation of streamflow and evapotranspiration (Govindaraju & Kavvas, 1991; Scudeler et al., 2017). The 2D simulated fluxes are converted into 3D fluxes by using a multiplicative factor  $l_m$  [L] :  $l_m = A/L$  where  $A$  is the basin area [ $L^2$ ] and  $L$  the hillslope length [L]. Moreover, in order to take into account the travel time through the river network, the critical depth outflow is used as input of a routing reservoir whose outflow is defined as a linear function of the water storage. The time parameter associated is obtained by calibration on the 3D simulated recession periods.

Soil parameters are identical to the ones used in the 3D model. Regarding hillslope vegetation parameters, they are obtained by computing weighted averages according to the basin surface occupied by each vegetation type. Equivalent hillslope geomorphic parameters (length  $L$  and slope  $\tan(\gamma)$ ) are based on both the LWW geomorphic analysis presented in section 2 and a manual calibration. The mean value of length distribution is retained as the equivalent length parameter:  $L=1200$  m. Manual calibration reveals that a slope parameter of  $\tan(\gamma) = 1\%$  allows the simulation of the 3D reference result with higher accuracy than the computed mean slope of 2%. This adjusted value is retained as the equivalent slope parameter.

Note that hillslope simulations are initialized using the same spin-up strategy as for 3D simulation.

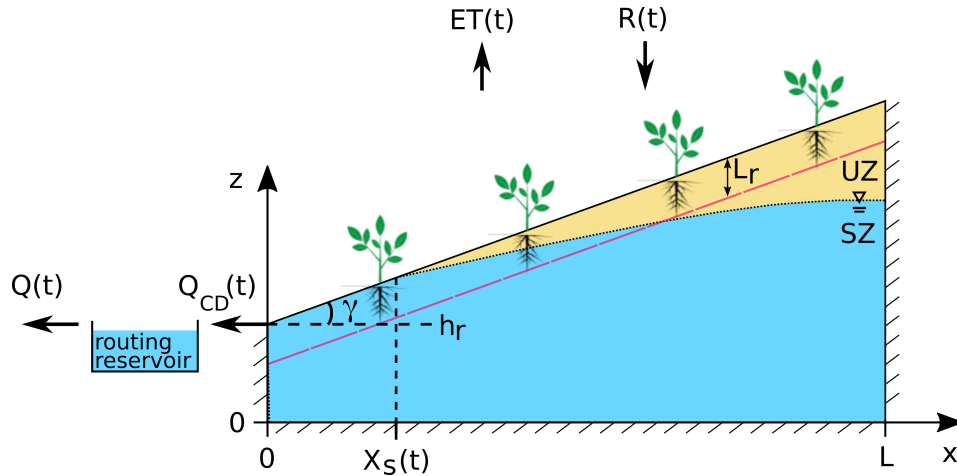


**Figure 4.** Scheme of the equivalent hillslope model at time  $t$ , which is characterized by its length  $L$  and its slope  $\tan(\gamma)$ .  $Q_{CD}(t)$  [ $L^3T^{-1}$ ] is the water discharge through the critical depth boundary condition,  $Q(t)$  [ $L^3T^{-1}$ ] is the discharge leaving the routing reservoir,  $R(t)$  [ $L^3T^{-1}$ ] is the rainfall,  $ET(t)$  [ $L^3T^{-1}$ ] is the evapotranspiration,  $X_s(t)$  [L] is the seepage face extension,  $h_r$  is the subsurface depth below the river and  $L_r$  is the root zone depth. Saturated zone (SZ) is represented in blue and unsaturated zone (UZ) in yellow.

264           **3.3 The Two-Hydrologic-Variable Analytical Model**

265           **3.3.1 Discharge**

266       Unconfined groundwater flow with a seepage outflow boundary condition is not an  
 267       easy problem to solve analytically. Most of the solutions invoke Dupuit assumption and  
 268       apply to steady flow in a dam type domain (Harr, 1991). A classical solution is obtained  
 269       by solving the 1D Dupuit equation with a boundary condition stating that the slopes  
 270       of both water table and soil are equal at their intersection point. This point defines the  
 271       seepage extension. For aquifer type domains (Figure 4) the Dupuit assumption still holds  
 272       for a domain of large lateral extension compared to the vertical one (Bresciani et al., 2014).  
 273       Nevertheless, below the river, in the region close to the no flow vertical boundary, the  
 274       flow is 2D and Dupuit assumption is no more valid. Moreover, when vegetation is taken  
 275       into account, the equality of soil and water table slopes is not verified. For these two rea-  
 276       sons, and also because we consider transient flow, we assume in our model that the wa-  
 277       ter table elevation varies linearly and makes an angle  $\tan(i(t))$  [–] (Figure 5). This as-  
 278       sumption has proved to be efficient in describing water table dynamics in small catch-  
 279       ments (Maquin et al., 2017). The water table intersects soil surface at  $x = X_s(t)$ .

280       It comes from our assumptions that our model depends on two variables :  $\tan(i(t))$   
 281       and  $X_s(t)$ . These two variables are linked but establishing their relationship is an issue  
 282       which is out of the scope of the paper. Therefore, we consider here that their evolution  
 283       are given by the numerical simulation.

284       Discharge is obtained by assuming the conservation of mass in the compartment  
 285       from  $x = 0$  to  $x = h_r$  (Figure 5a). Indeed,  $x = h_r$  can be considered as the limit where  
 286       the subsurface vertical flow becomes 2D. Dupuit assumption is used to compute the lat-  
 287       eral flow through the vertical section at  $x = h_r$ , whose length is approximated with  $h_r$ .  
 288       It corresponds to the baseflow  $Q_b(t)$  [ $L^3T^{-1}$ ]:

$$Q_b(t) = \begin{cases} Kh_r \tan(i(t)) & \text{if } X_s(t) \leq h_r \\ Kh_r \tan(\gamma) & \text{if } X_s(t) > h_r \end{cases} \quad (1)$$

289       A second process contributing to the streamflow is the saturation overland flow (Dunne  
 290       & Black, 1970), noted  $Q_{sof}$  [ $L^3T^{-1}$ ]. It is dependent on the seepage face extension  $X_s(t)$ ,  
 291       where net precipitation directly participates:

$$Q_{sof}(t) = [R(t) - E_{can}(t)]X_s(t) \quad (2)$$

292       with  $R(t)$  [ $LT^{-1}$ ] the rainfall rate and  $E_{can}(t)$  [ $LT^{-1}$ ] the evaporation rate from canopy,  
 293       computed in the same way as in the HGS code.

294       According to the computed mass balance, the hillslope total streamflow  $Q_H(t)$  is  
 295       given by:

$$Q_H(t) = Q_b(t) + Q_{sof}(t) - ET_{h_r}(t) \quad (3)$$

296       with  $ET_{h_r}(t)$  [ $L^3T^{-1}$ ] the evapotranspiration computed on the section from  $x = 0$  to  
 297        $x = h_r$  with the evapotranspiration analytical model described hereafter.

298           **3.3.2 Evapotranspiration**

299       Evapotranspiration is the sum of plant transpiration, subsurface and surface evap-  
 300       oration, and canopy evaporation. The PET is the maximum evapotranspiration rate. Evap-  
 301       otranspiration fluxes are computed by dividing the hillslope into four compartments ac-  
 302       cording to the linear water table position and its intersection with the root system (Fig-  
 303       ure 5b). The first compartment is defined by the seepage face where the subsurface is  
 304       fully saturated, i.e. where soil moisture and root distribution are not limiting factors for

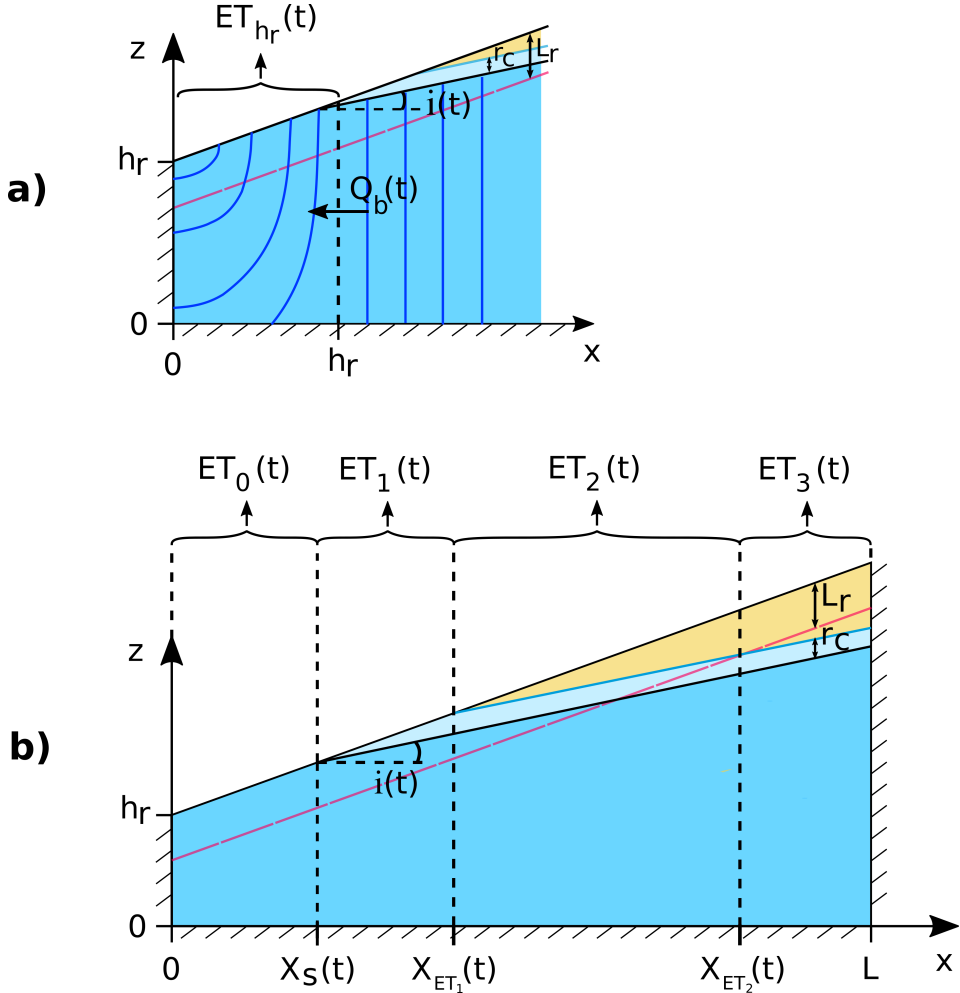


**Figure 5.** Analytical model scheme representing the variables involved in the computed a) discharge (eq. (1) to (3)) and b) evapotranspiration (eq. (3) to (7)). Saturated zone is represented in blue, capillarity zone in pale blue and the remaining unsaturated zone in yellow.

the transpiration, allowing the maximum rate of transpiration  $T_{r_{max}}(t)$  [ $LT^{-1}$ ] to occur. The evaporation rate  $E_{v_{X_s}}(t)$  [ $LT^{-1}$ ] is computed as the mean value between zero and the remaining evapotranspiration capacity ( $PET(t) - E_{can}(t) - T_{r_{max}}(t)$ ). The evapotranspiration rate in the first compartment  $ET_0(t)$  [ $LT^{-1}$ ] is given by:

$$ET_0(t) = T_{r_{max}}(t) + E_{v_{X_s}}(t) + E_{can}(t) \quad (4)$$

with

$$T_{r_{max}}(t) = [PET(t) - E_{can}(t)]f(LAI)(t) \quad (5)$$

$$E_{v_{X_s}}(t) = [(PET(t) - E_{can}(t)) - T_{r_{max}}(t)]/2 \quad (6)$$

where  $f(LAI)(t)$  [–] is the leaf area index function as computed in the HGS code.

In the other compartments, a capillary rise from the linear water table is considered by assuming hydrostatic equilibrium. The length  $r_c$  [ $L$ ] corresponds to the capillary rise from the water table (where  $\theta = \omega$  with  $\omega$  the porosity), to the height where  $\theta = (\theta_{fc} - \theta_{wp})/2$  with the field capacity water content  $\theta_{fc}$  and the wilting point water content  $\theta_{wp}$ . The second compartment is located between  $x = X_s(t)$  and  $x = X_{ET_1}(t)$

where the considered capillarity rise intersects land surface (Figure 5b). Water content in this compartment is not enough to allow evaporation but is assumed to still allow the maximum rate of transpiration. The resulting evapotranspiration rate  $ET_1(t)$  [ $LT^{-1}$ ] is given by:

$$ET_1(t) = T_{r_{max}}(t) + E_{can}(t) \quad (7)$$

In the third compartment, located between  $x = X_{ET_1}(t)$  and  $x = X_{ET_2}(t)$  (Figure 5b), evapotranspiration rate  $ET_2(t)$  [ $LT^{-1}$ ] is defined with:

$$ET_2(t) = T_{r_{max}}(t)RDF(t) + T_{r_{max}}(t)f(\theta)(t)(1 - RDF(t)) + E_{can}(t) \quad (8)$$

where  $RDF(t)$  is the root density function integrated on the volume including both saturated zone and capillarity zone. Soil moisture is assumed not to be limiting for transpiration in this volume. This is not true for the remaining unsaturated volume, where the water content function  $f(\theta)(t)$  [–] is computed. The Richards equation would be required for the rigorous computation of the water content function. However in the scope of this article we use the more simple modeling approach of the Antecedent Precipitation Index (API) (Chevallier & Hyperbav, 1983).

The fourth compartment evapotranspiration rate  $ET_3(t)$  [ $LT^{-1}$ ] is assumed not to be influenced by the water table, what gives:

$$ET_3(t) = T_{r_{max}}(t)f(\theta)(t) + E_{can}(t) \quad (9)$$

Finally, the hillslope total evapotranspiration  $ET_H(t)$  [ $L^3T^{-1}$ ] is given by:

$$ET_H(t) = \sum_{n=0}^3 (ET_n(t)\Delta X_n(t)) \quad (10)$$

where:

$$\begin{aligned} \Delta X_0(t) &= X_s(t) \\ \Delta X_1(t) &= X_{ET_1}(t) - X_s(t) \\ \Delta X_2(t) &= X_{ET_2}(t) - X_{ET_1}(t) \\ \Delta X_3(t) &= L - X_{ET_2}(t) \end{aligned}$$

Following this model, the evapotranspiration term  $ET_{hr}(t)$  involved in the calculation of the discharge (Equation 3) is given by:

$$ET_{hr}(t) = \begin{cases} ET_0(t)h_r & \text{if } X_s(t) \geq h_r \\ ET_0(t)X_s(t) + ET_1(t)(h_r - X_s(t)) & \text{if } X_s(t) < h_r \end{cases} \quad (11)$$

## 4 Results and Discussion

### 4.1 Three-Dimensional Reference Simulation Over the 1993-2013 Period

The ability of the three-dimensional integrated model to simulate the actual long term water budget of the LWW is assessed by comparing simulated and measured streamflows at USGS1 station and latent heat flux at the Ameriflux site (locations represented in Figure 1). As previously shown, USGS1 streamflow data are available during the whole period. Regarding latent heat flux measurement, the campaign took place from January 1997 to December 1998 (Meyers, 2016).

Figure 6 shows the comparison between simulated and measured discharges at USGS1. The three-dimensional reference result is validated on measured discharge using the Kling-Gupta efficiency (KGE) criteria (Gupta et al., 2009). It results from the decomposition

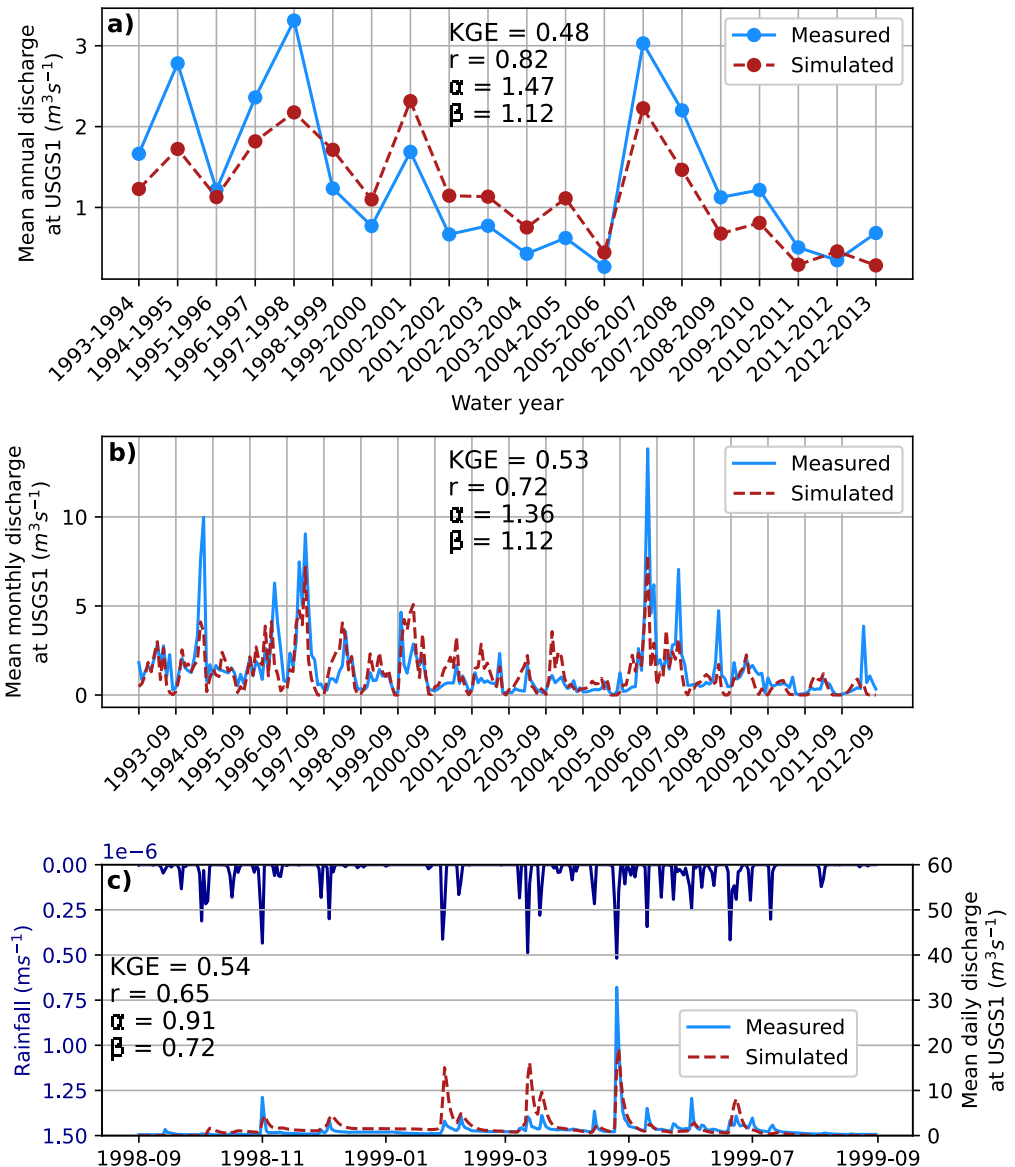


**Figure 6.** (a) Mean annual and (b) monthly discharge at USGS1 station over the 20-year period and (c) daily discharge during the 1998–1999 water year: comparison of measured data and 3D reference simulation results.

of the Nash-Sutcliffe efficiency (NSE) criteria. This decomposition into three components is known for offering a complete interpretation of the bias:  $r$  represents the linear correlation coefficient,  $\alpha$  is the variability ratio, computed using the standard deviation, and  $\beta$  is the ratio between data means. Ideal value for KGE and its components is 1. Comparison between simulated and measured mean annual discharges at USGS1 shows a good simulation of the decreasing tendency over the 20-year period (Figure 6a). Although general tendency is well reproduced by the model, discrepancies are noticeable: annual discharge is underestimated over the periods 1993 to 1998 and 2007 to 2011 while it is over-

estimated between 1998 and 2006. By looking at monthly means (Figure 6b), it appears that for some years, the first half of the water year is well simulated while the second half is underestimated by the model (1994-1995 for instance). However, for the other years, first half of the water year is overestimated while second half is well simulated (1998-1999 for instance). Different factors can explain the difficulties of the model to capture the seasonal cycle and its variability over 20 years : the spatial and temporal resolutions of PET and rainfall forcings, or the constancy of evapotranspiration parameters. Indeed, Li et al. (2008) show the importance of adjusting these parameters from one year to another, since evapotranspiration fluxes rely on empirical relationships. A close up is done on the 1998-1999 water year, which is the one simulated by Kollet and Maxwell (2008), in order to evaluate the model at the daily timescale (Figure 6c): as noticed previously, the model has difficulties to capture the variation of seasonality from one year to another, leading in 1998-1999 to both baseflow and peak flow rates overestimated from December to April. However, the plotted hydrograph shows a good fitness of the model to capture peak flow timing.

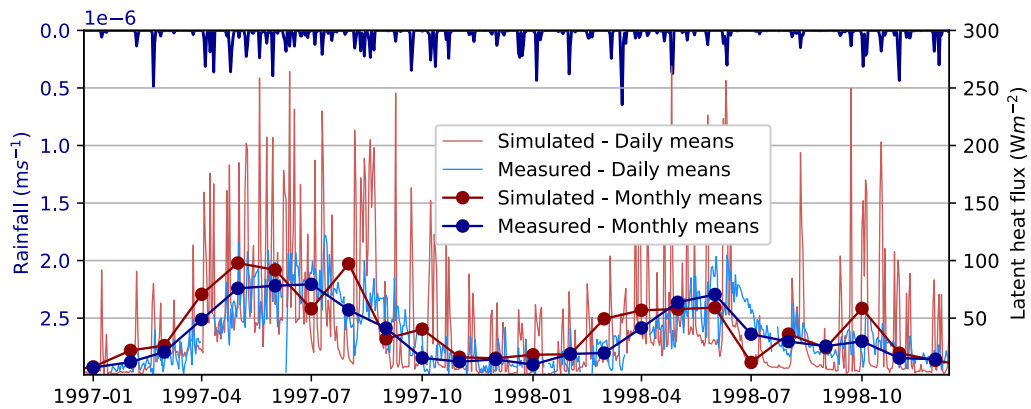


**Figure 7.** Comparison of latent heat fluxes measured at the Ameriflux site and simulated at the 3D mesh closest node.

The ability of the model to simulate evapotranspiration fluxes is tested through the comparison of latent heat fluxes simulated and measured at the Ameriflux site. At this location, the model horizontal resolution is around 1000 m. Latent heat flux simulated at the closest node is plotted in Figure 7 along with the measured one. This plot shows a good agreement when looking at monthly means. However, daily data show a simulated variation amplitude up to three times higher than the measured one. These simulated peaks with a high amplitude correspond to simulated evaporation from canopy. Indeed, in the HGS code, the minimum between potential evapotranspiration and rainfall rate is considered as evaporated from the canopy, leading in our case to disparities with measured data. Nevertheless, this result should be treated cautiously since the Ameriflux measurement tower provides a very local dataset that is here compared to the flux simulated at one node in a mesh which horizontal resolution is approximately 1000 m.

As a result, the comparison of the reference three-dimensional simulation with available measured data highlights some model limitations. However, the major tendencies are reasonably well captured with KGE values approaching 0.5 for the simulated discharge. Moreover, the fit on the 1998-1999 water year is comparable to what is obtained in the literature. These results are consequently considered satisfactory enough to serve as reference for the following modeling steps.

356

## 4.2 Comparison with the 2D Equivalent Hillslope Model

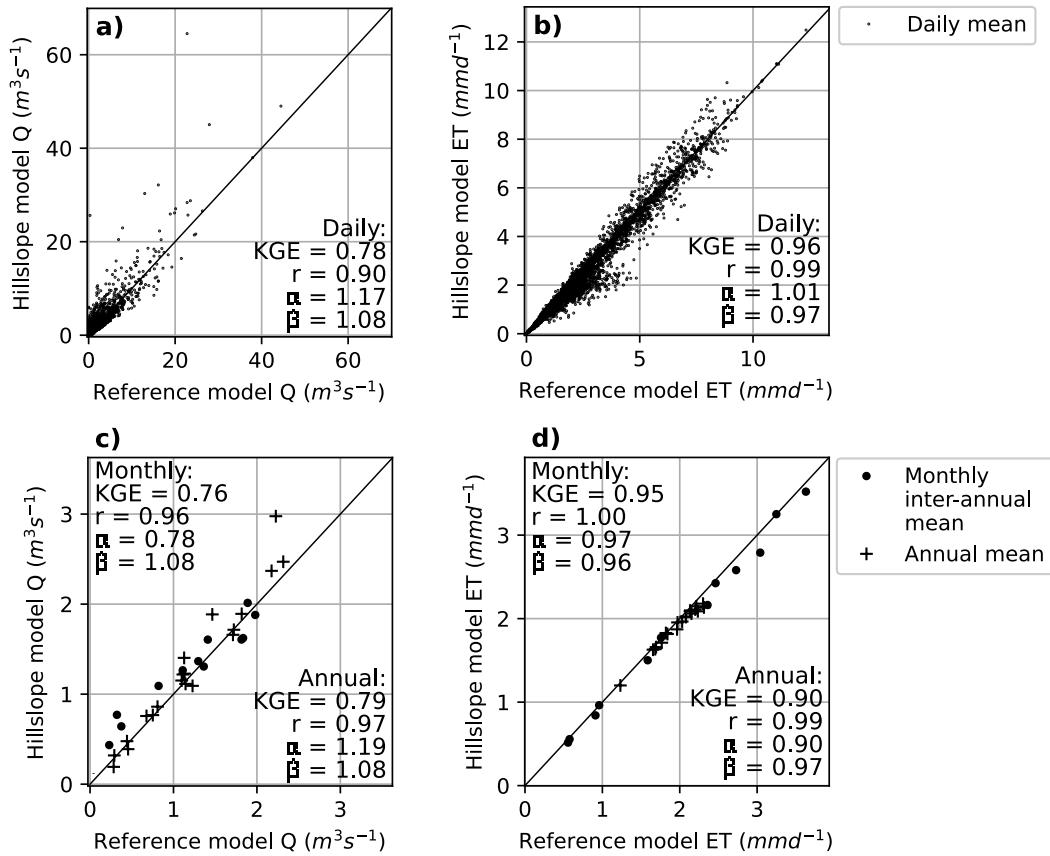


**Figure 8.** Comparison between 2D equivalent hillslope and 3D reference simulation of the discharge at the outlet station USGS1 (a and c), and the ET over the whole basin (b and d): Daily means (a and b) and annual and monthly inter-annual means over the 20 years (c and d).

357  
358  
359  
360  
361  
362  
363  
364  
365  
366  
367  
368  
369

Equivalent hillslope model capacity to reproduce the three-dimensional reference result is quantified using the previously described Kling-Gupta efficiency criteria (KGE). Results are shown in Figure 8 for the two outgoing fluxes: the discharge  $Q$  (Figures 8a and 8c) and the evapotranspiration  $ET$  (Figures 8b and 8d). Fluxes evolution over the 20 years is investigated at three timescales by looking at daily means, monthly inter-annual means and annual means, allowing a complete comparison of the models behaviours. First regarding the discharge, KGE values are respectively 0.78, 0.76 and 0.79 for the three timescales, what describes a strong correlation between discharge simulated with equivalent hillslope and reference models. This correlation is even stronger between the simulated ET fluxes with KGE values of 0.96, 0.95 and 0.90. In conclusion, the LWW 3D simulated water balance is captured by the equivalent hillslope model with good accuracy, however a greater accuracy loss occurs on the discharge (KGE values approaching 0.8) than on the ET (KGE values greater than or equal to 0.9).

370  
371  
372  
373

Figure 9 shows results concerning the simulation of a local variable: the depth to water table ( $d2WT [L]$ ) at the closest nodes from river network (i.e. 100m far from the river, according to the spatial resolution). In 3D, averaged  $d2WT$  is computed on nodes groups in which local slope equals a given slope  $\tan(\gamma) \pm 0.5\%$ . Local slope is defined

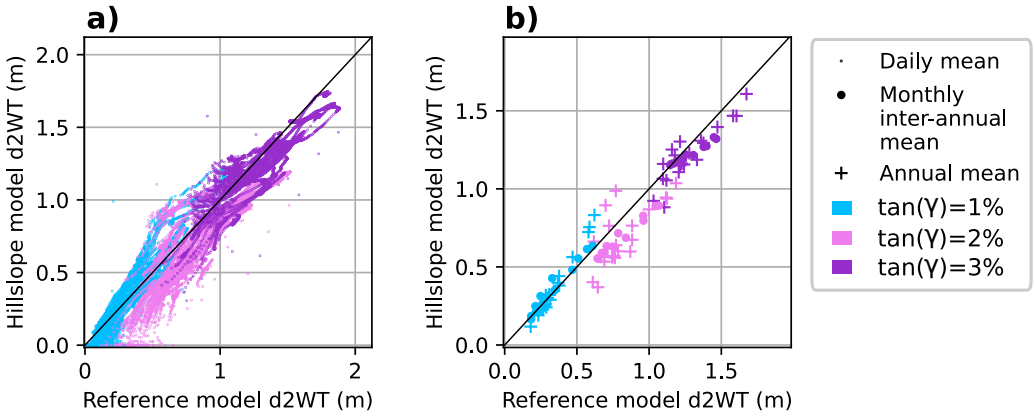


**Figure 9.** Evaluation of the hillslope model for the simulation of 3D local long term water table depth evolution ( $d2WT [L]$ ): The 3D mesh nodes located around the river network are regrouped according to the soil surface angle  $\tan(\gamma)$  they form with the closest river node. Mean water table depth is calculated for each group and compared with water table depth simulated with a hillslope model having the same  $\tan(\gamma)$  parameter. Figure (a) shows the scatter plot of daily means over the 20 years and Figure (b) shows the scatter plot of annual and monthly inter-annual means.

as the soil surface angle between each node and its closest downstream river node. This way, 3D simulated  $d2WT$  are computed for  $\tan(\gamma)$  of 1%, 2%, and 3%. Nodes with a local slope from 0.5% to 3.5% are consequently considered here, what represents 80% of the 3D nodes located at 100 m around the river network. Two-dimensional simulations are run on hillslope models having the same  $\tan(\gamma)$  parameter ( $L$  is still set to 1200 m). Simulated depth to water table at  $x = 100$  m is compared with the one simulated on 3D nodes. For each slope, hillslope model reproduces the 3D local water table depth evolution with good accuracy: KGE values calculated on daily means over the whole period are equal or higher than 0.65. This result demonstrates the capacity of a hillslope model to not only reproduce the 3D simulated basin's water budget but also the local water table dynamics. The slope of the equivalent hillslope model is 1%. The local water table dynamic simulated by the equivalent hillslope model is therefore comparable to the one simulated in 3D hillslopes with local slopes of  $1 \pm 0.5\%$ . These slopes represent 40% of 3D local slopes around the river network, what could justify the slope parameter of the equivalent hillslope model.

#### 4.3 The Two-Variable Analytical Model: Qualification and Comparison with the Equivalent Hillslope Model

The analytical model is first qualified by analysing its response to different hillslope geometry parameters. Then, the discharge and the evapotranspiration given by the analytical model are compared to those simulated with the equivalent hillslope model over the 20-year period.

##### 4.3.1 Analytical Model Response to the Hillslope Geometry

Analytical model (referred to as AM) response to various hillslope geometry parameters is analysed by conducting hillslope numerical and analytical simulations over one year with a set of length and slope values. Considered length values range from 400 m to 5000 m, and slope values range from 0.8% to 2.8%, what includes the means (1200

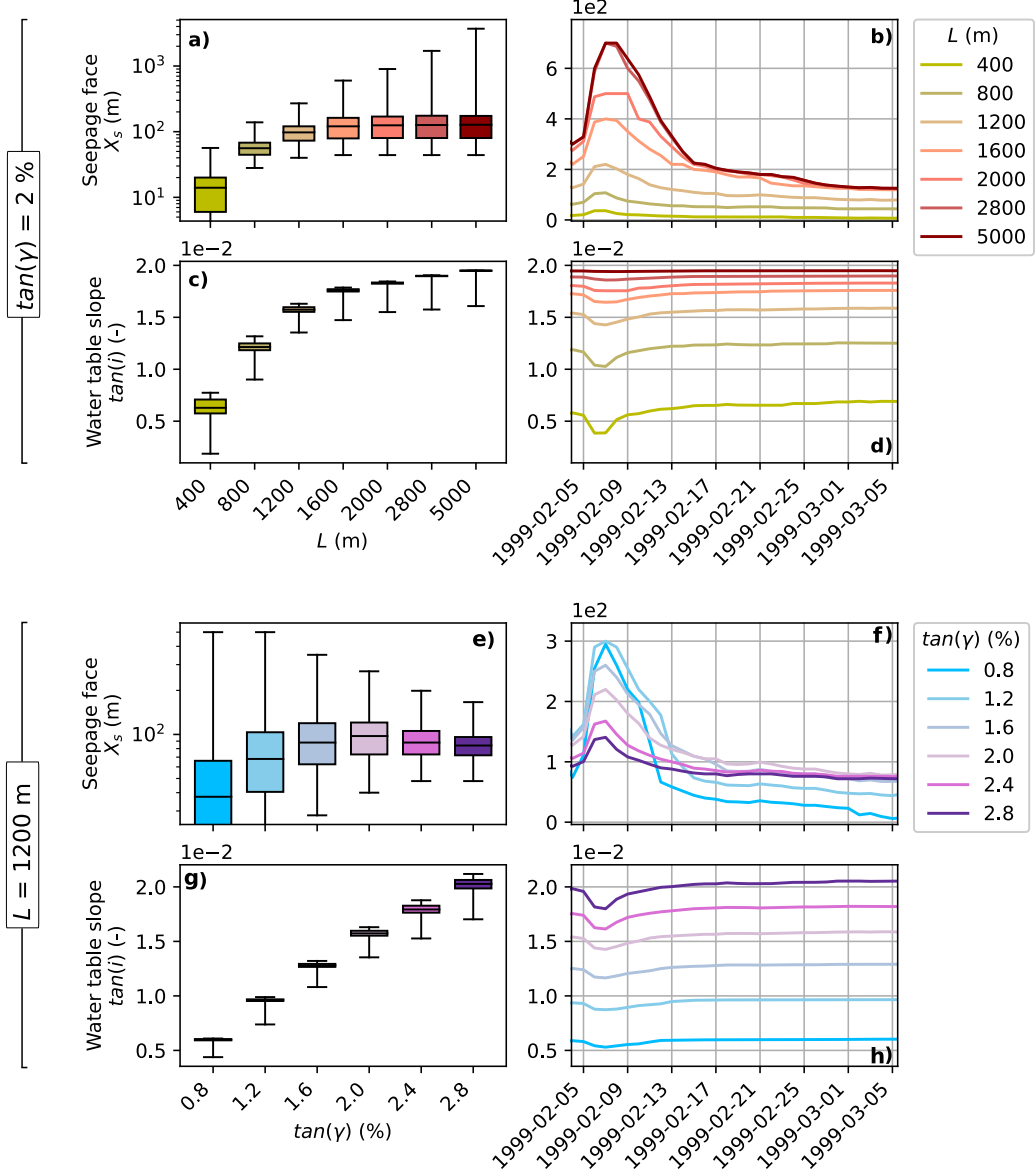


**Figure 10.** Hillslope model: Evolution of (a, b, e, f) seepage face extension  $X_s$ , and (c, d, g, h) water table slope  $\tan(i)$  with (a-d) different hillslope lengths  $L$  (and a constant slope of 2%) and with (e-h) different slopes  $\tan(\gamma)$  (and a constant length of 1200 m). Plots a, c, e, and g are boxplots of daily values for each parameter value over the 1998-1999 water year, while b, d, f and h plots show daily values during February 1999 including a rainfall event of  $1.3 \times 10^{-7} \text{ ms}^{-1}$ . Boxplots middle lines indicate median values, boxplots extensions indicate the range between first and third quartiles, and whiskers extend to extreme data. Note that the y-axis of seepage face extension boxplots are plotted on a logarithmic scale.

400 m and 2%) and also include 60% of the hillslope lengths and slopes found in the basin  
 401 (Figures 2a and 2b). In order to accurately observe the seepage face extension  $X_s(t)$  and the water table slope  $\tan(i(t))$  responses to different hillslope geometry parameters, hill-  
 402 slope model (referred to as HM) simulations are conducted with refined grid meshes. One  
 403

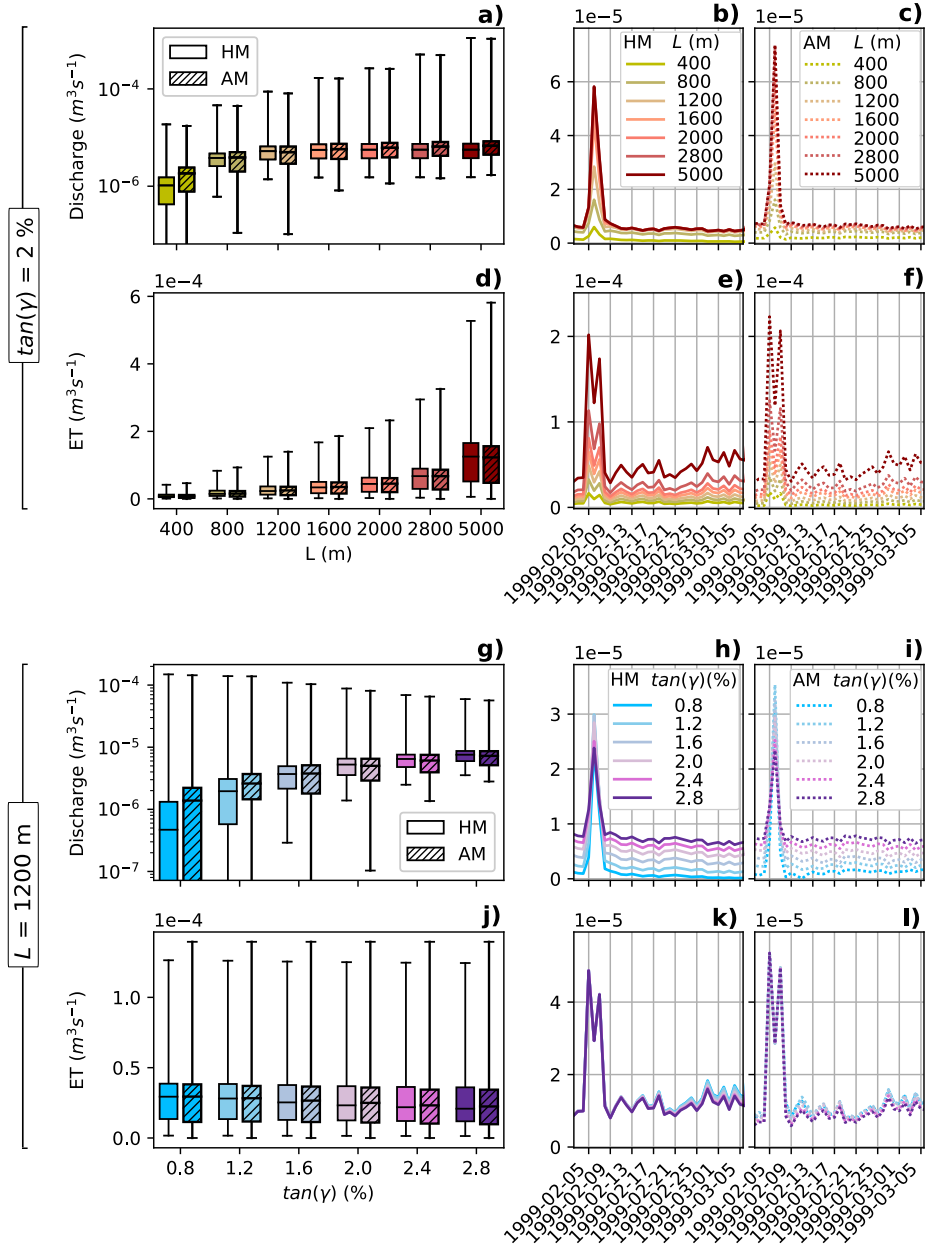


**Figure 11.** Comparison of hillslope model (HM) and analytical model (AM) simulated (a-c, g-i) discharges and (d-f, j-l) evapotranspiration fluxes with (a-f) different hillslope lengths  $L$  (and a constant slope of 2%) and with (g-l) different slopes  $\tan(\gamma)$  (and a constant length of 1200 m). Plots a, d, g and j show a comparison of HM and AM boxplots of daily values for each parameter value over the 1998-1999 water year. Plots b, e, h and k show HM daily values during February 1999 including a rainfall event of  $1.3 \times 10^{-7} m s^{-1}$  while c, f, i and l plots show the same results simulated with AM. Boxplots middle lines indicate median values, boxplots extensions indicate the range between first and third quartiles, and whiskers extend to extreme data. Note that the y-axis of discharge boxplots are plotted on a logarithmic scale.

404 year evolution of the simulated  $X_s(t)$  and  $\tan(i(t))$  are plotted in Figure 10 for differ-  
405 ent values of  $L$  and  $\tan(\gamma)$ .

406 Results show that both  $X_s(t)$  and  $\tan(i(t))$  increase as length expands, until con-  
407 verging (Figures 10a-10d)). Water table slope tends towards  $\tan(\gamma)$  (Figures 10c and 10d)  
408 while  $X_s(t)$  reaches a median value around 100 m (Figure 10a). Moreover an enlarge-  
409 ment of  $X_s(t)$  variability with  $L$  is shown by the whiskers extension. In conclusion, as  
410  $L$  increases the water table gets closer to the soil surface what produces a seepage face  
411 extension more sensible to rainfall events.

412 In the same way, evolution of  $X_s(t)$  and  $\tan(i(t))$  with  $\tan(\gamma)$  is shown in Figures  
413 10e to 10h. A quasi linear water table slope increase is observable as the soil slope in-  
414 creases (Figures 10g and 10h). Regarding  $X_s$  evolution with slope, the expected result  
415 would be a decrease of the intersection surface between groundwater and soil surface as  
416 the slope increases. However, the inverse tendency is observed for the median  $X_s$  value  
417 for slopes between 0.8% and 2.0% (Figure 10e). It is explained by the large interaction  
418 volume between root zone and water table when soil surface slope approaches zero. Veg-  
419 etation uptake leads to short  $X_s$  recession times (Figure 10f) and can result in a seep-  
420 age face disappearance (minimum  $X_s$  value equals to zero for slopes of 0.8% and 1.2%  
421 in Figure 10e).

422 The associated discharge and evapotranspiration simulated with both the HM and  
423 the AM are compared in Figure 11. As  $L$  increases, HM median discharge value increases  
424 and tends to a maximum limit, while the whiskers (i.e. the variability) increases (Fig-  
425 ure 11a). It results from the water table gradient tending to its maximum value of  $\tan(\gamma)$ ,  
426 what causes: 1. A maximum baseflow and 2. A seepage face extension which is highly  
427 sensitive to rainfall events and thus creates high peak flow rates with saturated overland  
428 flow (Figure 11b). By involving  $X_s$  and  $\tan(i)$ , the AM is able to well capture these pro-  
429 cesses (Figures 11a and 11c). KGE indexes are computed between the AM and HM re-  
430 sults. Regarding the simulated discharge for the different hillslope lengths, KGE values  
431 between the two models are equal or higher than 0.71. As expected, the HM evapotran-  
432 spiration increases with  $L$  because of: 1. The enlargement of surface for canopy evapo-  
433 ration that creates larger evaporated volumes during precipitations. 2. The expansion  
434 of the intersection volume between the saturated zone and the root zone, enhancing larger  
435 transpired volumes. This rise is also well captured by the AM with KGEs equal or higher  
436 than 0.87 (Figures 11d-11f).

437 The impacts of the slope parameter on the HM and the AM simulated discharges  
438 and evapotranspiration fluxes are plotted in Figures 11g to 11l. A rise in the HM dis-  
439 charge median values with  $\tan(\gamma)$  is noticeable while the whiskers are shortened (Fig-  
440 ure 11g). It is the result of the water gradient rise with soil surface slope and the seep-  
441 age face decreasing variability. Indeed these phenomena respectively cause a baseflow  
442 increase and a decreasing variability of saturated overland flow (Figure 11 (B)h). Again,  
443 the AM is able to capture these processes since it depends on the two driving variables  
444  $X_s$  and  $\tan(i(t))$  (Figure 11g and 11i). KGE indexes are computed to compare the AM  
445 and HM results. KGE indexes computed on the discharge with the different slopes are  
446 equal or higher than 0.83. Regarding the evapotranspiration, the HM median value slightly  
447 decreases with  $\tan(\gamma)$  (Figure 11j). Indeed a drop of  $ET$  occurs particularly in high at-  
448 mospheric demand periods, and is the result of water table position: as hillslope gets steeper,  
449 a smaller volume of water is accessible to the vegetation. KGE indexes computed be-  
450 tween the HM and AM simulated ET with the different slopes are equal or higher than  
451 0.96. This good agreement demonstrates the ability of the analytical model to capture  
452 the hillslope model evapotranspiration fluxes whatever the slope.

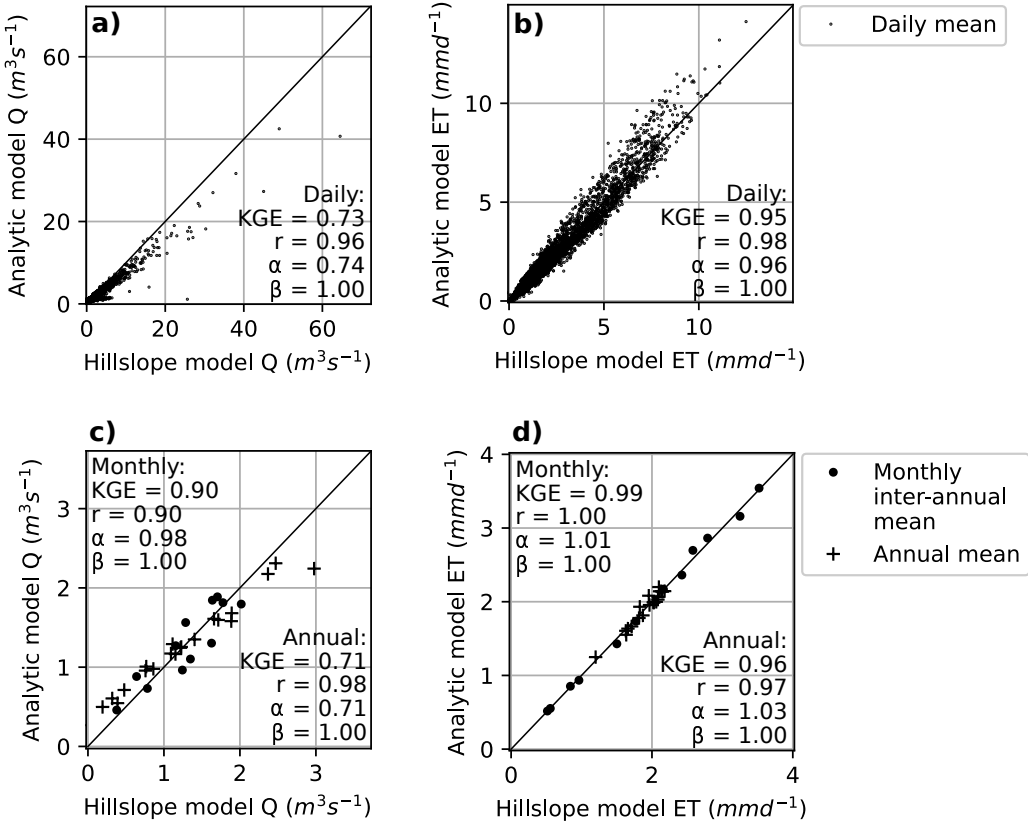


**Figure 12.** Comparison between the analytical model (AM) and the 2D equivalent hillslope model simulations of the discharge at the outlet station USGS1 (a and c), and the ET over the whole basin (b and d): Daily means (a and b) and annual and monthly inter annual means over the 20 years (c and d).

#### 4.3.2 Comparison with the Equivalent Hillslope Model

Basin's water balance simulated with the 2D equivalent hillslope model (with equivalent parameters  $L = 1200$  m and  $\tan(\gamma) = 1\%$ ) over the 20-year period is compared to the basin's water balance simulated with the two-variable analytical model AM. Results are shown in Figure 12. Evapotranspiration fluxes are very well captured by the analytical model, with KGE values of 0.95, 0.99 and 0.96 for respectively daily, monthly and annual means. Hypothesis allowing the computation of analytical discharge lead to a higher accuracy loss, however the AM ability to capture the basin's discharge can still be qualified as good with KGE values of 0.73, 0.90 and 0.71. As a result, the 2D LWW equivalent hillslope water balance is captured with reasonable accuracy by the two-variable analytical model. By extension, the analytical model simulates the 3D LWW reference water balance with reasonable accuracy.

These satisfactory results are explained by the essential role of  $X_s(t)$  and  $\tan(i(t))$  on which the AM depends. As described in section 3.3.1, the discharge is produced by two processes: the baseflow that is driven by the hydraulic gradient  $\tan(i(t))$ , and the saturation overland flow that occurs on  $X_s(t)$ . Regarding the evapotranspiration, it directly depends on the available soil water content for the root system. This water content is provided in two ways: by the groundwater storage and its capillary rise and by the rainfall infiltration. The proportion of groundwater and rainwater in the evapotran-

472 spiration fluxes depends on the position of the water table, which is described by  $X_s(t)$   
 473 and  $\tan(i(t))$ . In conclusion, knowing the evolution of these two variables over time al-  
 474 lows us to describe the different processes at the origin of the water balance.

## 475 5 Conclusion

476 In response to the current challenge of improving the representation of hydrology  
 477 in Land Surface Models (LSMs), we propose an upscaling approach based on the dimen-  
 478 sionality reduction of the 3D watershed processes. The objective is to identify the hy-  
 479 drologic variables that govern the watershed water mass balance and need to be imple-  
 480 mented into LSMs.

481 The Little Washita Watershed is selected as an experimental site for the develop-  
 482 ment of our approach, since its size is close to that of a LSM grid cell, and since it com-  
 483 piles lot of experimental and modeling studies. First a 3D physically-based model of the  
 484 watershed is built with the HydroGeoSphere integrated code (HGS) in order to have a  
 485 space and time continuous view on the basin's hydrology that will serve as a reference.  
 486 The 3D simulation of 20-year hydrology is considered to capture experimental measured  
 487 discharge and evapotranspiration fluxes with enough accuracy to be used as a reference.  
 488 Then, the hillslope being considered as the main hydrologic unit controlling main lat-  
 489 eral flows and water availability for evapotranspiration, a 2D equivalent hillslope model  
 490 is built with HGS. This model is shown to be able to reproduce both 3D simulated wa-  
 491 ter balance and local water table dynamics with good accuracy. Finally, hillslope phys-  
 492 ical processes are conceptualized through simplifying assumptions (Dupuit and linear wa-  
 493 ter table assumptions). It leads to the identification of two driving variables: the seep-  
 494 age face extension and the water table slope. An analytical model integrating these two  
 495 variables is proposed. This model relies on the water balance of different hillslope com-  
 496 parts and describes the discharge and evapotranspiration related processes. The anal-  
 497 ytical model is qualified in two steps. First, the results are compared with those of the  
 498 HGS hillslope model for different values of slope and length. It shows the ability of the  
 499 analytical model to capture the water balance of a hillslope model, whatever its geom-  
 500 etry. Then, the results are compared with those of the equivalent hillslope model over  
 501 the 20-year period of time. It shows the good capacity of the analytical model to com-  
 502 pute the water balance of the equivalent hillslope model, and therefore of the reference  
 503 3D watershed model, over the 20 years.

504 As a result, the model dimensionality is reduced from the reference 3D model to  
 505 the 2D equivalent hillslope model, and from the equivalent hillslope model to an ana-  
 506 lytical model based on two driving variables. These variables play a key role since they  
 507 allow the computation of baseflow and saturation overland flow, and they provide infor-  
 508 mation on the distribution along the hillslope of the groundwater available for evapo-  
 509 transpiration. For the purpose of this paper the two variables are taken from the numer-  
 510 ical simulation and injected into the analytical model. The next step of the model de-  
 511 velopment will be to establish a relationship between these two variables and write the  
 512 hillslope water mass conservation as a function of one of the variables. Though the model  
 513 has been qualified on different hillslope geometries it will need to be tested on different  
 514 types of watershed. Finally, the work presented in this paper shows that discharge and  
 515 evapotranspiration are governed by different hillslope reservoirs, also called compartments  
 516 in the paper. In the bottom-up strategy adopted here, this naturally leads to the ques-  
 517 tion of how to embed these reservoirs, which lateral extensions vary with time and where  
 518 flow dimension varies laterally, into the one-dimensional columns models used in LSMs?

## 519 Acknowledgments

520 This work was funded by the LEFE program of the French National Center for Scien-  
 521 tific Research (CNRS/INSU). The authors would like to thank René Therrien (Univer-

522 sité Laval, Quebec, Canada) for supporting this work. The LWW geomorphic analysis  
 523 data, the HGS simulation files (run files, parameter files and output files) for both 3D  
 524 reference model and equivalent hillslope model, and the python code of the analytical  
 525 model are available at <https://doi.org/10.5281/zenodo.5289921> (Picourlat et al.,  
 526 2021).

## 527 References

- 528 Allen, P., & Naney, J. (1991). Hydrology of little washita river watershed: Okla-  
 529 homa—data and analyses, ars-90. *Agric. Res. Serv. US Dep. of Agric., Durant,*  
 530 *Okla.*
- 531 Band, L. E. (1989). Spatial aggregation of complex terrain. *Geographical Analysis*,  
 532 *21*(4), 279–293.
- 533 Bixio, A., Gambolati, G., Paniconi, C., Putti, M., Shestopalov, V., Bublias, V., ...  
 534 Rudenko, Y. (2002). Modeling groundwater-surface water interactions in-  
 535 cluding effects of morphogenetic depressions in the chernobyl exclusion zone.  
*Environmental Geology*, *42*(2-3), 162–177.
- 536 Bonan, G. B., Oleson, K. W., Vertenstein, M., Levis, S., Zeng, X., Dai, Y., ... Yang,  
 537 Z.-L. (2002). The land surface climatology of the community land model  
 538 coupled to the ncar community climate model. *Journal of climate*, *15*(22),  
 539 3123–3149.
- 540 Bresciani, E., Davy, P., & de Dreuzy, J.-R. (2014). Is the dupuit assumption suitable  
 541 for predicting the groundwater seepage area in hillslopes? *Water Resources*  
 542 *Research*, *50*(3), 2394–2406.
- 543 Caddo county climate summary [Computer software manual]. (2017). Re-  
 544 trieval from [http://ocs.mesonet.org/county\\_climate/Products/](http://ocs.mesonet.org/county_climate/Products/)  
 545 *County\_Climatologies/county\_climate\_caddo.pdf*
- 546 Camporese, M., Paniconi, C., Putti, M., & Orlandini, S. (2010). Surface-subsurface  
 547 flow modeling with path-based runoff routing, boundary condition-based cou-  
 548 pling, and assimilation of multisource observation data. *Water Resources*  
 549 *Research*, *46*(2).
- 550 Chaney, N. W., Metcalfe, P., & Wood, E. F. (2016). Hydroblocks: a field-scale re-  
 551 solving land surface model for application over continental extents. *Hydrologi-  
 552 cal Processes*, *30*(20), 3543–3559.
- 553 Chevallier, P., & Hyperbav, G. (1983). Antecedent precipitation index. estimation of  
 554 soil on moisture representative catchments. *Cahiers ORSTOM Serie hydrolo-  
 555 gie*.
- 556 Clark, M. P., Bierkens, M. F., Samaniego, L., Woods, R. A., Uijlenhoet, R., Bennett,  
 557 K. E., ... Peters-Lidard, C. D. (2017). The evolution of process-based hydro-  
 558 logic models: historical challenges and the collective quest for physical realism.  
*Hydrology and Earth System Sciences*, *21*(7), 3427–3440.
- 559 Clark, M. P., Fan, Y., Lawrence, D. M., Adam, J. C., Bolster, D., Gochis, D. J., ...  
 560 others (2015). Improving the representation of hydrologic processes in earth  
 561 system models. *Water Resources Research*, *51*(8), 5929–5956.
- 562 Condon, L. E., & Maxwell, R. M. (2014). Feedbacks between managed irrigation  
 563 and water availability: Diagnosing temporal and spatial patterns using an  
 564 integrated hydrologic model. *Water Resources Research*, *50*(3), 2600–2616.
- 565 Dunne, T., & Black, R. D. (1970). Partial area contributions to storm runoff in a  
 566 small new england watershed. *Water Resources Research*, *6*(5), 1296–1311.
- 567 Fan, Y., & Bras, R. L. (1998). Analytical solutions to hillslope subsurface storm flow  
 568 and saturation overland flow. *Water Resources Research*, *34*(4), 921–927.
- 569 Fan, Y., Clark, M., Lawrence, D. M., Swenson, S., Band, L., Brantley, S. L., ... oth-  
 570 ers (2019). Hillslope hydrology in global change research and earth system  
 571 modeling. *Water Resources Research*, *55*(2), 1737–1772.
- 572

- 574 Ferguson, I. M., & Maxwell, R. M. (2010). Role of groundwater in watershed re-  
 575 sponse and land surface feedbacks under climate change. *Water Resources Re-*  
 576 *search*, 46(10).
- 577 Fisher, R. A., & Koven, C. D. (2020). Perspectives on the future of land surface  
 578 models and the challenges of representing complex terrestrial systems. *Journal*  
 579 *of Advances in Modeling Earth Systems*, 12(4), e2018MS001453.
- 580 Freeze, R. A., & Harlan, R. (1969). Blueprint for a physically-based, digitally-  
 581 simulated hydrologic response model. *Journal of Hydrology*, 9(3), 237–258.
- 582 Garbrecht, J. D., Zhang, X., & Steiner, J. L. (2014). Climate change and observed  
 583 climate trends in the fort cobb experimental watershed. *Journal of Environ-*  
 584 *mental Quality*, 43(4), 1319–1327.
- 585 Govindaraju, R. S., & Kavvas, M. L. (1991). Dynamics of moving boundary over-  
 586 land flows over infiltrating surfaces at hillslopes. *Water Resources Research*,  
 587 27(8), 1885–1898.
- 588 Gupta, H. V., Kling, H., Yilmaz, K. K., & Martinez, G. F. (2009). Decomposi-  
 589 tion of the mean squared error and nse performance criteria: Implications for  
 590 improving hydrological modelling. *Journal of hydrology*, 377(1-2), 80–91.
- 591 Harr, M. E. (1991). *Groundwater and seepage*. Courier Corporation.
- 592 Hazenberg, P., Broxton, P., Gochis, D., Niu, G.-Y., Pangle, L., Pelletier, J., ...  
 593 Zeng, X. (2016). Testing the hybrid-3-d hillslope hydrological model in a  
 594 controlled environment. *Water Resources Research*, 52(2), 1089–1107.
- 595 Hazenberg, P., Fang, Y., Broxton, P., Gochis, D., Niu, G.-Y., Pelletier, J., ... Zeng,  
 596 X. (2015). A hybrid-3d hillslope hydrological model for use in earth system  
 597 models. *Water Resources Research*, 51(10), 8218–8239.
- 598 Horton, R. E. (1932). Drainage-basin characteristics. *Eos, Transactions American*  
 599 *Geophysical Union*, 13(1), 350–361.
- 600 Hrachowitz, M., & Clark, M. P. (2017). Hess opinions: The complementary merits  
 601 of competing modelling philosophies in hydrology. *Hydrology and Earth System*  
 602 *Sciences*, 21(8), 3953–3973.
- 603 Khan, U., Tuteja, N. K., Ajami, H., & Sharma, A. (2014). An equivalent cross-  
 604 sectional basis for semidistributed hydrological modeling. *Water Resources Re-*  
 605 *search*, 50(5), 4395–4415.
- 606 Kollet, S. J., & Maxwell, R. M. (2008). Capturing the influence of groundwater  
 607 dynamics on land surface processes using an integrated, distributed watershed  
 608 model. *Water Resources Research*, 44(2).
- 609 Kristensen, K., & Jensen, S. (1975). A model for estimating actual evapotranspira-  
 610 tion from potential evapotranspiration. *Hydrology Research*, 6(3), 170–188.
- 611 Li, Q., Unger, A., Sudicky, E. A., Kassenaar, D., Wexler, E., & Shikaze, S. (2008).  
 612 Simulating the multi-seasonal response of a large-scale watershed with a 3d  
 613 physically-based hydrologic model. *Journal of Hydrology*, 357(3-4), 317–336.
- 614 Loritz, R., Hassler, S. K., Jackisch, C., Allroggen, N., Schaik, L. v., Wienhöfer, J.,  
 615 & Zehe, E. (2017). Picturing and modeling catchments by representative  
 616 hillslopes. *Hydrology and Earth System Sciences*, 21(2), 1225–1249.
- 617 Maquin, M. (2016). *Développement d'un modèle hydrologique de colonne*  
 618 *représentant l'interaction nappe-végétation-atmosphère et applications à*  
 619 *l'échelle du bassin versant* (Unpublished doctoral dissertation). Université  
 620 Paris-Saclay (ComUE).
- 621 Maquin, M., Mouche, E., Mügler, C., Pierret, M.-C., & Viville, D. (2017). A soil  
 622 column model for predicting the interaction between water table and evapo-  
 623 transpiration. *Water Resources Research*, 53(7), 5877–5898.
- 624 Maxwell, R. M., Condon, L. E., & Kollet, S. J. (2015). A high-resolution simulation  
 625 of groundwater and surface water over most of the continental us with the in-  
 626 tegrated hydrologic model parflow v3. *Geoscientific Model Development*, 8(3),  
 627 923–937.

- 628 Maxwell, R. M., Kollet, S. J., Smith, S. G., Woodward, C. S., Falgout, R. D., Ferguson, I. M., ... Ashby, S. (2009). Parflow user's manual. *International Ground*  
 629 *Water Modeling Center Report GWMI*, 1 (2009), 129.
- 630 Mesinger, F., DiMego, G., Kalnay, E., Mitchell, K., Shafran, P. C., Ebisuzaki, W.,  
 631 ... others (2006). North american regional reanalysis. *Bulletin of the Ameri-*  
 632 *can Meteorological Society*, 87(3), 343–360.
- 633 Meyers, T. (2016). *Ameriflux us-lww little washita watershed* (Tech. Rep.). Ameri-  
 634 Flux; NOAA/ARL.
- 635 Milly, P. C., Malyshev, S. L., Shevliakova, E., Dunne, K. A., Findell, K. L., Gleeson,  
 636 T., ... Swenson, S. (2014). An enhanced model of land water and energy  
 637 for global hydrologic and earth-system studies. *Journal of Hydrometeorology*,  
 638 15(5), 1739–1761.
- 639 Moriasi, D. N., Starks, P. J., Steiner, J. L., Guzman, J. A., Allen, P. B., & Naney,  
 640 J. W. (2014). Upper washita river experimental watersheds: physiography  
 641 data. *Journal of Environmental Quality*, 43(4), 1298–1309.
- 642 Nijssen, B., Lettenmaier, D. P., Liang, X., Wetzel, S. W., & Wood, E. F. (1997).  
 643 Streamflow simulation for continental-scale river basins. *Water Resources*  
 644 *Research*, 33(4), 711–724.
- 645 Picourlat, F., Mouche, E., & Mügler, C. (2021, August). *Capturing the Little*  
 646 *Washita watershed water balance with a physically-based two-hydrologic-*  
 647 *variable model*. Zenodo. Retrieved from <https://doi.org/10.5281/zenodo.5289921> doi: 10.5281/zenodo.5289921
- 648 Rigon, R., Bertoldi, G., & Over, T. M. (2006). Geotop: A distributed hydrological  
 649 model with coupled water and energy budgets. *Journal of Hydrometeorology*,  
 650 7(3), 371–388.
- 651 Rosero, E., Gulden, L. E., Yang, Z.-L., De Goncalves, L. G., Niu, G.-Y., & Kaheil,  
 652 Y. H. (2011). Ensemble evaluation of hydrologically enhanced noah-lsm:  
 653 Partitioning of the water balance in high-resolution simulations over the little  
 654 washita river experimental watershed. *Journal of Hydrometeorology*, 12(1),  
 655 45–64.
- 656 Rosnay, P. d., & Polcher, J. (1998). Modelling root water uptake in a complex  
 657 land surface scheme coupled to a gcm. *Hydrology and Earth System Sciences*,  
 658 2(2/3), 239–255.
- 659 Scudeler, C., Paniconi, C., Pasetto, D., & Putti, M. (2017). Examination of the  
 660 seepage face boundary condition in subsurface and coupled surface/subsurface  
 661 hydrological models. *Water Resources Research*, 53(3), 1799–1819.
- 662 Starks, P. J., Fiebrich, C., Grimsley, D., Garbrecht, J. D., Steiner, J. L., Guzman,  
 663 J. A., & Moriasi, D. N. (2014). Upper washita river experimental watersheds:  
 664 Meteorologic and soil climate measurement networks. *Journal of Environmen-*  
 665 *tal Quality*, 43(4), 1239–1249.
- 666 Starks, P. J., Steiner, J. L., & Stern, A. (2014). Upper washita river experimental  
 667 watersheds: Land cover data sets (1974–2007) for two southwestern oklahoma  
 668 agricultural watersheds. *Journal of environmental quality*, 43(4), 1310–1318.
- 669 Steiner, J. L., Starks, P. J., Garbrecht, J. D., Moriasi, D. N., Zhang, X., Schneider,  
 670 J. M., ... Osei, E. (2014). Long-term environmental research: The upper  
 671 washita river experimental watersheds, oklahoma, usa. *Journal of Environmen-*  
 672 *tal Quality*, 43(4), 1227–1238.
- 673 Swenson, S. C., Clark, M., Fan, Y., Lawrence, D. M., & Perket, J. (2019). Rep-  
 674 resenting intrahillslope lateral subsurface flow in the community land model.  
 675 *Journal of Advances in Modeling Earth Systems*, 11(12), 4044–4065.
- 676 Therrien, R., McLaren, R., Sudicky, E. A., & Panday, S. (2010). Hydrogeosphere: A  
 677 three-dimensional numerical model describing fully-integrated subsurface and  
 678 surface flow and solute transport. *Groundwater Simulations Group, University*  
 679 *of Waterloo, Waterloo, ON*.

- 682 Tootchifatidehi, A. (2019). *Development of a global wetland map and application*  
683 *to describe hillslope hydrology in the orchidee land surface model* (Unpublished  
684 doctoral dissertation). Sorbonne Université.
- 685 Troch, P. A., Paniconi, C., & Emiel van Loon, E. (2003). Hillslope-storage boussi-  
686 nesq model for subsurface flow and variable source areas along complex hill-  
687 slopes: 1. formulation and characteristic response. *Water Resources Research*,  
688 39(11).
- 689 Van Liew, M. W., & Garbrecht, J. D. (2003). Hydrologic simulation of the little  
690 washita river experimental watershed using swat 1. *JAWRA Journal of the*  
691 *American Water Resources Association*, 39(2), 413–426.
- 692 Verbeke, T., Tootchi, A., Jost, A., Ghattas, J., Cheruy, F., & Ducharme, A. (2019).  
693 Subgrid-scale parametrization of groundwater-soil moisture interactions in  
694 the orchidee land surface model: first results at global scale. In *Geophysical*  
695 *research abstracts* (Vol. 21).
- 696 Wigmosta, M. S., Vail, L. W., & Lettenmaier, D. P. (1994). A distributed  
697 hydrology-vegetation model for complex terrain. *Water Resources Research*,  
698 30(6), 1665–1679.